Analysis and DSP Implementation of a Broadband Duct ANC System Using Spatially Feedforward Structure

Mingsian R. Bai

Yujeng Lin

Department of Mechanical Engineering,
National Chiao-Tung University,
1001 Ta-Hsueh Road,
Hsin-Chu 300, Taiwan,
Republic of China

Jian-Da Wu

Department of Vehicle
Engineering & Technology,
Da-Yeh University,
112 Shan-Jeau Road,
Da-Tsuen, Chang-Hwa 515, Taiwan,
Republic of China

The active control technique for broadband attenuation of noise in ducts, using spatially feedforward structure, is investigated from the viewpoints of both acoustic analysis and control engineering. According to the previous work by Munjal and Eriksson [1], there exists an ideal controller for this problem. The ideal controller is a function of the finite source impedance and is thus independent of the boundary conditions. Despite the simplicity, the ideal controller cannot be practically implemented due to the difficulty of calibration of electro-mechanical parameters. To overcome the problem, the controller is implemented via an equivalent formulation modified from the controller originally proposed by Roure [2]. The modified controller is implemented on a DSP platform, using a FIR filter, an IIR filter and a hybrid filter. The experimental results showed that the system achieved 17.2 dB maximal attenuation in the frequency band 300~600 Hz. Physical insights and design considerations in implementation phase are also discussed in the paper. [DOI: 10.1115/1.1355031]

1 Introduction

Active noise control (ANC) techniques have attracted much research attention because they provide numerous advantages over conventional passive methods in attenuating low frequency noises [3]. In the ANC applications to date, feedforward control has been widely used whenever nonacoustical reference is available [4]. However, if nonacoustical reference is not available but the order of the system is small, e.g., the headset problem, feedback control should be a feasible approach [5]. Feedback control by colocated sensors and actuators results in a passive, positive real and thus minimum phase plant [6,7]. The phase response of such a system always alternates between ± 90 deg. Stability is guaranteed because of the passivity [8]. In practical implementation, however, the positive real (PR) property may no longer exist due to in-band transducer dynamics. As a crucial step in the feedback design, certain phase compensation schemes may be needed to alleviate this nonpositive real problem [9].

In the other extreme of high-order systems, conventional feedback control generally achieves only narrowband attenuation due to *spillover effect* [7,10]. In this paper, a more preferable structure, the *spatially feedforward structure* (Fig. 1(*a*)) is exploited for high-order systems, where nonacoustical reference is unavailable and broadband attenuation is desired. It has been demonstrated in Hong and Bernstein's paper [7] that the spatially feedforward structure suffers less from the spillover problem than the colocated feedback structure.

In the spatially feedforward control structure, a measurement sensor is placed near the noise source but far away from the control source. The measurement sensor measures the sound from not only the noise source but also the control source (the latter is called *acoustic feedback path* that generally causes undesirable effects). From the viewpoint of control theory, the structure *per se* is not feedforward since nonacoustic disturbance is not accessible. This is hence the reason why we use the term ''spatially feedforward.'' It shares the same design constraints on performance, stability and robustness as the other classical feedback systems.

For the spatially feedforward structure, Munjal and Eriksson [1] derived an ideal ANC controller based on acoustic filter theory. The ideal controller is a function of the finite source impedance only and is thus independent of the upstream and downstream conditions. This paper seeks to provide an in-depth acoustic analysis of an ideal controller for ducts and details of how to implement it. Using electro-mechanical analogy, the ideal controller is extended to incorporate the transducer dynamics. However, after several attempts, the ideal controller still cannot be implemented due to the errors in calibrating electro-mechanical parameters. To overcome the difficulty, the controller is implemented

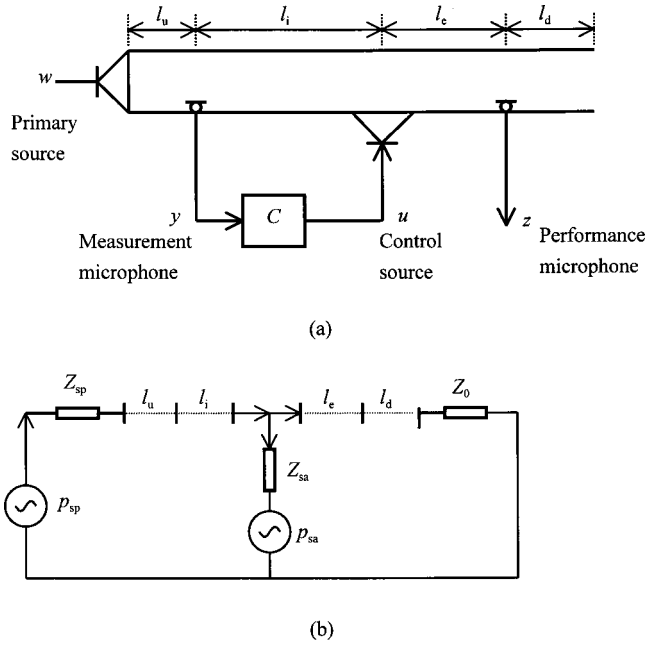

Fig. 1 Spatially feedforward structure (*a*) schematic of the duct ANC system (*b*) equivalent circuit

Contributed by the Technical Committee on Vibration and Sound for publication in the JOURNAL OF VIBRATION AND ACOUSTICS. Manuscript received July 1999; revised Oct. 2000. Associate Editor: R. L. Clark.

via an equivalent formulation modified from the original controller proposed by Roure [2]. The modified controller is implemented on a DSP platform, using a FIR filter, an IIR filter and a hybrid filter. The experimental results showed that the proposed system achieved broadband attenuation of the noise in a duct. The design considerations in practical implementations are also discussed in the paper.

2 Analysis of the Ideal Controller for Ducts

The spatially feedforward ANC system for a duct and its equivalent circuit are shown in Fig. 1. Based on the concept of acoustic short-circuit, Munjal and Eriksson [1] derived an ideal controller capable of achieving global noise cancellation downstream the control source in a finite-length duct:

$$C_{ideal} = -\frac{Z_{sa}}{Y_0}\left(\frac{e^{-jkl_1}}{1-e^{-2jkl_i}}\right) = C_{EM}\cdot C_{RP}, \tag{1}$$

where Z_{sa} is the acoustic impedance of the control source, $Y_0 = c/S$ is the characteristic impedance of the duct, c is the sound speed, S is the cross sectional area of the duct, k is wavenumber, and l_i is the distance between the upstream measurement microphone and the control source. This ideal controller is an infinite-dimensional controller and no modal truncation was made. In Eq. (1),

$$C_{EM} \equiv -\frac{Z_{sa}}{Y_0} \tag{2}$$

is a function of the finite impedance Z_{sa} which depends only on the electro-mechanical constants of the control source. On the other hand,

$$C_{RP} \equiv \frac{e^{-jkl_i}}{1-e^{-2jkl_i}} \tag{3}$$

exhibits an interesting form of a *repetitive controller* [11] which periodically reproduces any finite duration input signal. Its frequency response and impulse response both show equally spaced peaks ($\Delta f = c/2l_i$, $\Delta t = 2l_i/c$). If the system contains no damping, the poles will be on the imaginary axis and the repetitive controller is unstable. These unstable poles are introduced due to acoustic feedback. At the pole frequencies, the controller exerts high gain because the measurement sensor is at the pressure node. In reality, absorption effect of ducts is always present (such as the wooden duct in our case) and the wave number k becomes complex. The poles of repetitive controller will be in the open left-half space and the controller is stable. However, for lightly damped duct and omni-directional transducers, the controller can be marginally stable and the impulse response can be unacceptably long. To avoid the adverse effect of acoustic feedback, directional transducers or arrays can be used [12,13].

From Eq. (1), some interesting features are noted. For a feedback structure ($l_i = 0$), $C_{ideal} \to \infty$, which implies colocated feedback control is an impractical approach for global attenuation. Secondly, the controller is applicable to all frequencies and is thus a broadband controller. In particular, the controller produces maximal attenuation at the resonances of the duct field. Third, the ideal controller is independent of the conditions upstream the reference microphone and downstream the control source such as the primary source impedance and radiation impedance. This provides an advantage in practical applications in which a universal, detachable ANC module can be developed for various kinds of operational conditions. It is also noted that the performance of attenuation still depends on boundary conditions, although the form of ideal controller remains unique.

3 Implementation of Practical Controllers

3.1 Method of Electro-mechanical Constants. From Eq. (1), the implementation of the ideal controller requires the knowledge of the control source impedance Z_{sa}. In what follows, Z_{sa} will be expressed explicitly in terms of speaker parameters.

Figure 2(*a*) shows an electro-mechanical equivalent circuit of a moving-coil loudspeaker [14]. In the figure, e_g is the open-circuit voltage of the generator; R is the total equivalent resistance of the coil; L is the equivalent inductance of the coil; Bl is the coil constant; u_c is the cone velocity; f_c is the force produced by the coil; z_M is the mechanical mobility. Reflecting all elements, e_g, R and L, to the mechanical side yields Fig. 2(*b*). Let Ω be the analog frequency. The ''blocked'' ($u_c = 0$) force is

$$f_c|_{u_c=0} = \frac{e_g/Bl}{\frac{R}{B^2l^2} + j\Omega\frac{L}{B^2l^2}} = \frac{e_g Bl}{R + j\Omega L}, \tag{4}$$

whereas the ''free'' ($f_c = 0$) velocity is

$$u_c|_{f_c=0} = \frac{e_g}{Bl}\frac{z_M}{\frac{R}{B^2l^2} + j\Omega\frac{L}{B^2l^2} + z_M}. \tag{5}$$

Thus, Z_{sa} can be expressed as

$$Z_{sa} = \frac{1}{\rho S^2}\frac{f_c|_{u_c=0}}{u_c|_{f_c=0}} = \frac{1}{\rho S^2}\left(\frac{1}{z_M} + \frac{B^2l^2}{R + j\Omega L}\right). \tag{6}$$

As expected, Z_{sa} depends solely on speaker parameters R, L and Bl which can be identified in advance by some existing (but often not trivial) procedures, e.g., Bai and Wu [15].

In addition to the speaker dynamics, the characteristics of the microphone and the power amplifier must be taken into account such that the input and output of the controller involve only electrical voltages. Referring to Fig. 3, the controller to implement is defined as

$$C'_{ideal} \equiv \frac{e^s}{e_m}, \tag{7}$$

where e_m is the output voltage of the measurement microphone and e_s is the input voltage of the power amplifier. The loading effect in the microphone is negligible because the input impedance of the pre-amp is generally very large. Thus the microphone is assumed to have a constant gain g_m that can be obtained from the microphone vendor. Hence,

$$e_m = g_m p_m, \tag{8}$$

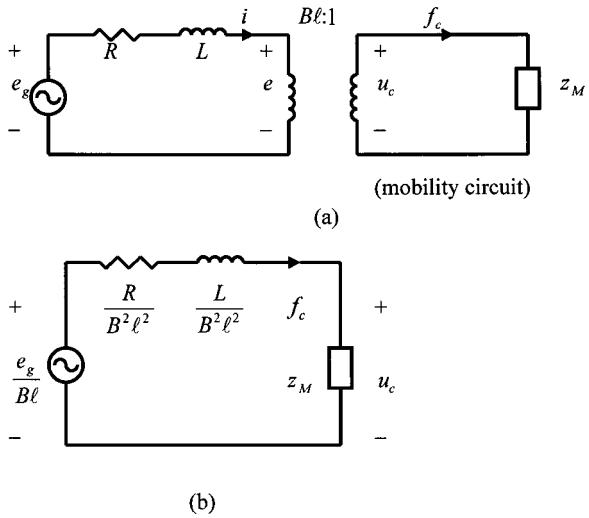

Fig. 2 Electro-mechanical analysis of a moving coil speaker (*a*) equivalent circuit with an ideal transformer (*b*) circuit reflected to the mechanical side

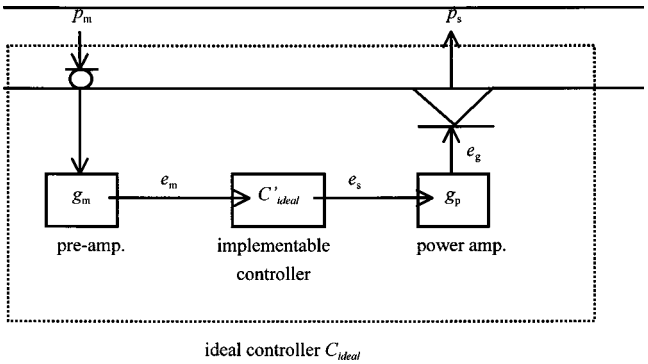

Fig. 3 The implementable controller involving only electrical voltages

where p_m is the input acoustic pressure of the microphone. From Eq. (4), it can be shown that speaker frequency response function

$$G_s \equiv \frac{p_s}{e_g} = \frac{Bl}{S(R+j\Omega L)}, \tag{9}$$

where p_s is the output acoustic pressure of the speaker. On the other hand, the power amplifier also has a constant gain g_p that can be determined by direct measurement

$$e_g = g_p e_s . \tag{10}$$

Combining Eq. (1), (7)–(10) yields

$$C'_{ideal} = -\frac{1}{G_{XDCR}}\left(\frac{e^{-jkl_i}}{1-e^{-2jkl_i}}\right), \tag{11}$$

where

$$G_{XDCR} = (g_p g_m G_s)\frac{Y_0}{Z_{sa}} \tag{12}$$

represents the overall transducer dynamics. Observation of Eq. (11) reveals an important fact: the transducer response must compete with the propagation delay e^{-jkl_i}, of the acoustic path. More precisely, the condition under which the resulting controller is causal is that the term e^{-jkl_i}/G_{XDCR} must be causal. This is an important causality constraint one must observe when the spatially feedforward structure is used.

The ideal controller of Eq. (11) was digitally implemented in an experiment. Unfortunately, the controller results in unstable response. The possible explanation of the outcome could be twofolded. First, the ideal controller is essentially of infinite band and excessive control output may saturate the system. Second, the error of identifying the electro-mechanical-acoustical parameters caused significant deviation of the system from the nominal plant. Therefore, we chose an equivalent but simpler approach originally proposed by Roure [2] to implement the ideal controller.

3.2 Roure's Controller. The spatially feedforward control can be represented by a block diagram in Fig. 4(*a*), where *w*, *y*, *z* and *u* are exogenous noise, measurement, performance variable and control input, respectively; the transfer functions *G*'s are self-explanatory from the subscripts. A so-called *zero spillover controller* [7] can be obtained by imposing the condition of perfect cancellation ($z=0$):

$$C_{ZSP}(j\Omega) = \frac{G_{zw}(j\Omega)}{G_{zw}(j\Omega)G_{yu}(j\Omega) - G_{zu}(j\Omega)G_{yw}(j\Omega)}. \tag{13}$$

A critical limitation of this controller is that it requires the knowledge of the disturbance-related transfer functions G_{zw} and G_{yw} which are generally unavailable in practice. To circumvent the problem, a more practical but equivalent controller proposed by Roure can be used. This is done by dividing the numerator and the denominator of Eq. (13) by $G_{yw}(j\Omega)$:

$$C_{ZSP}(j\Omega) = \frac{-\dfrac{G_{zw}(j\Omega)}{G_{yw}(j\Omega)}}{G_{zu}(j\Omega) - G_{yu}(j\Omega)\dfrac{G_{zw}(j\Omega)}{G_{yw}(j\Omega)}} = \frac{-H_0(j\Omega)}{H_2(j\Omega) - H_1(j\Omega)H_0(j\Omega)} \equiv C_{Roure}(j\Omega), \tag{14}$$

where

$$H_0(j\Omega) \equiv \frac{G_{zw}(j\Omega)}{G_{yw}(j\Omega)}, \tag{15}$$

is the frequency response function between the performance microphone and the measurement microphone,

$$H_1(j\Omega) \equiv G_{yu}(j\Omega) \tag{16}$$

is the frequency response function between the measurement microphone and the control speaker and

$$H_2(j\Omega) \equiv G_{zu}(j\Omega) \tag{17}$$

is the frequency response function between the performance microphone and the control speaker. All of these functions are measurable. In particular, $H_0(j\Omega)$ can be experimentally obtained by calculating the frequency response between the pressures measured at the performance microphone and the measurement microphone when the duct is excited by an upstream broadband random noise source. The block diagram of the Roure's controller is shown in Fig. 4(*b*).

Next, we will prove the equivalence between the zero spillover controller and the ideal controller. Using Munjal and Eriksson's [1] notations, the transfer functions, G_{yw}, G_{zw}, G_{yu}, and G_{zu} can be identified as

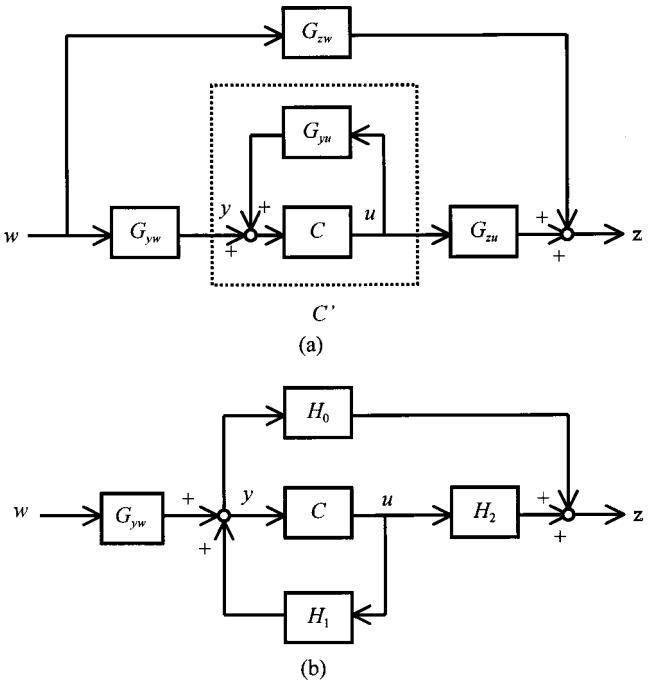

Fig. 4 Equivalent formulations of ideal controller (*a*) zero spillover controller (*b*) Roure's controller

$$G_{yw}=\frac{p_{5p}}{p_{spi}},\quad G_{zw}=\frac{p_{3p}}{p_{spi}},\quad G_{yu}=\frac{p_{5a}}{p_{sa}},\quad G_{zu}=\frac{p_{3a}}{p_{sa}}, \tag{18}$$

Using Munjal and Eriksson's [1] results and the definitions of Eq. (18), one can manipulate the zero spillover controller of Eq. (13) as follows:

$$\begin{aligned}
C_{ZSP}(j\Omega)&=\frac{G_{zw}(j\Omega)}{G_{zw}(j\Omega)G_{yu}(j\Omega)-G_{zu}(j\Omega)G_{yw}(j\Omega)}\\
&=\frac{\left[\frac{p_{3p}}{p_{spi}}\right]}{\left[\frac{p_{3p}}{p_{spi}}\right]\left[\frac{p_{5a}}{p_{sa}}\right]-\left[\frac{p_{3a}}{p_{sa}}\right]\left[\frac{p_{5p}}{p_{spi}}\right]}\\
&=\frac{\left[\frac{\zeta_e}{Z_{spi}VR}\right]}{\left[\frac{\zeta_e}{Z_{spi}VR}\right]\left[\frac{\zeta_e}{Z_{sa}VR}\right]-\left[\frac{\zeta_e}{Z_{sa}}\frac{C_i+jY_0S_i/Z_{spi}}{VR}\right]\left[\frac{\zeta_eC_i+jY_0S_i+jY_0S_i\zeta_e/Z_{sa}}{Z_{spi}VR}\right]}\\
&=\frac{Z_{sa}VR}{\zeta_e-(C_i+jY_0S_i/Z_{spi})(\zeta_eC_i+jY_0S_i+jY_0S_i\zeta_e/Z_{sa})}\\
&=\frac{Z_{sa}VR}{-jY_0S_iVR}\\
&=\frac{jZ_{sa}}{Y_0S_i}=-\frac{Z_{sa}}{Y_0}\left(\frac{e^{-jk_0l_i}}{1-e^{-2jk_0l_i}}\right)=C_{ideal}(j\Omega)
\end{aligned} \tag{19}$$

In light of the equivalence of the ideal controllers, one may thus conclude that the ideal controller for global attenuation downstream the control source can be replaced by Roure's controller which relies on only a single performance microphone.

It should be mentioned that the ideal controller could be noncausal and an approximate zero spillover controller must be implemented [7].

3.3 Implementation of the Roure's Controller. In the paper, digital implementation was employed. Every input-output relationship is expressed as a *z*-domain transfer function with its frequency response expressed as $G(e^{j\omega})=G(z)|_{z=e^{j\omega}}$, $\omega=\Omega T$ being the digital frequency with sampling period T.

First, we use Roure's original approach to implement the controller by a FIR filter. A sample frequency response of $C(e^{j\omega})$ in Eq. (15) obtained from experiments is shown in Fig. 5(*a*). To prevent the system from saturation, we multiply the frequency response function by a bandpass filter $W(e^{j\omega})$ whose pass band is our desired control bandwidth (300~600 in our case)

$$C'(e^{j\omega})=W(e^{j\omega})C(e^{j\omega}), \tag{20}$$

where $C'(e^{j\omega})$ represents Roure's controller filtered by the bandpass filter $W(e^{j\omega})$. Then the impulse response of Roure's controller, the coefficients of the FIR filter, can be obtained by taking inverse Fourier transform of Eq. (20) and then truncating the noncausal part, as shown in Fig. 5(*b*). It is noted that the filter $W(z)$ corrupts the phase of the ideal controller, which could cause performance degradation, and even instability. In reality, the effective bandwidth is somewhat less than expected, while instability rarely occurs because the controller gain is considerably attenuated outside control bandwidth and sufficient phase margin is preserved.

From the frequency response and the impulse response, the important features of the repetitive controller such as periodic peaks are readily observed. The equivalence of Roure's controller and Munjal's ideal controller is evidenced. Because the poles of the controller are lightly damped, the length of the resulting FIR filter is excessively large. This motivates the use of the following IIR implementation of the Roure's controller. Similar to the FIR implementation, we filter the frequency response function of Roure's controller by using a bandpass filter $W(e^{j\omega})$. Then we apply a frequency domain identification procedure [16] to obtain the transfer function $\hat{C}'(z)$ of the filtered controller which can be implemented by an IIR filter.

As the third approach of implementation, a hybrid structure is proposed in light of the physical structure revealed by the ideal controller. The main idea is to decompose Roure's controller $C(e^{j\omega})$ into a FIR part $C_{\mathrm{FIR}}(e^{j\omega})$ and an IIR part $C_{\mathrm{IIR}}(e^{j\omega})$

$$C(e^{j\omega})=C_{\mathrm{FIR}}(e^{j\omega})C_{\mathrm{IIR}}(e^{j\omega}). \tag{21}$$

The IIR part $C_{\mathrm{IIR}}(e^{j\omega})$ should display the pattern of a repetitive controller: periodic peaks in both frequency domain and time domain. On the other hand, $C_{\mathrm{FIR}}(e^{j\omega})$ represents transducer dynamics that is generally of low order and can be implemented by a FIR filter.

How can we find the IIR part of Roure's controller? A straightforward method is to match the frequency response of the controller with the repetitive controller. However, this proved to be an unsuccessful attempt because of the errors at the resonances. Alternatively, we chose to find second order systems, $C_1(e^{j\omega})\sim C_n(e^{j\omega})$, to match peaks within the control bandwidth (Fig. 6). Then, we cascade these second order systems to get $C_{\mathrm{IIR}}(e^{j\omega})$

$$C_{\mathrm{IIR}}(e^{j\omega})=C_1(e^{j\omega})C_2(e^{j\omega})\cdots C_n(e^{j\omega}) \tag{22}$$

which can be implemented by an IIR filter. Care should be taken to choose the gain level of each stage of second-order system such that no overflow or underflow problem would occur. Hence, the remaining part of Roure's controller, $C_{\mathrm{FIR}}(e^{j\omega})$, can be expressed as

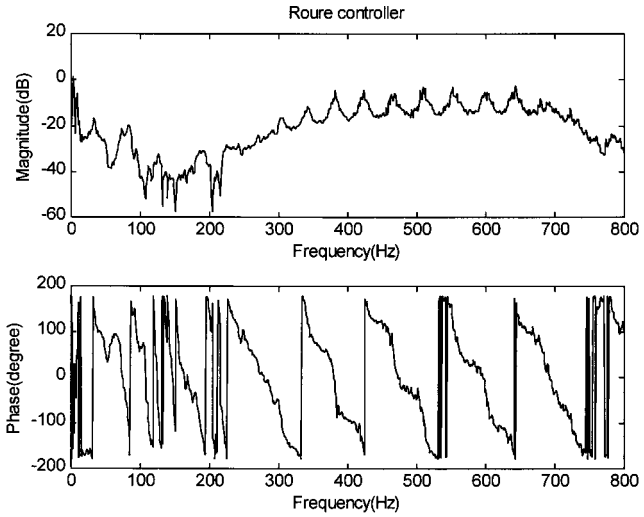

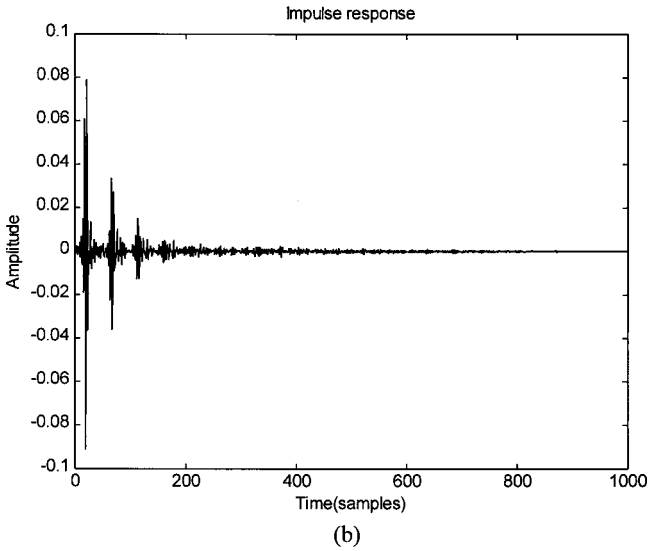

Fig. 5 Roure's controller (*a*) frequency response function (*b*) impulse response function

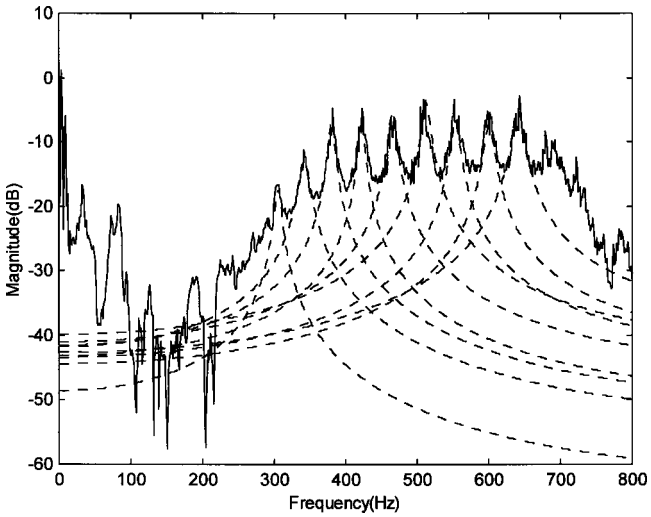

Fig. 6 Second order filters of hybrid implementation —: Roure's controller - -: second order filters

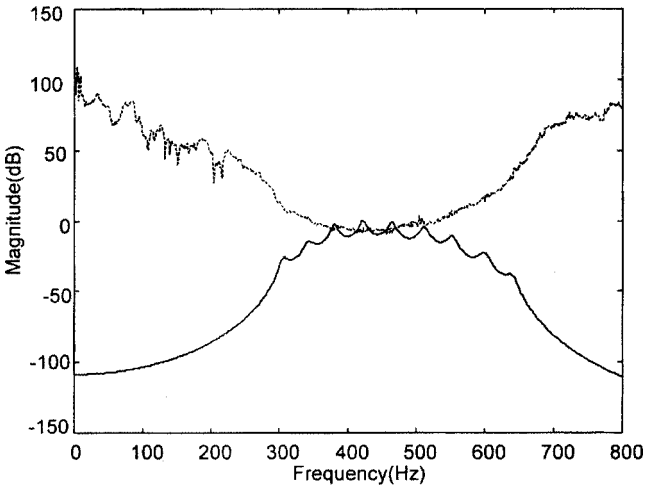

Fig. 7 Frequency response functions of $C_{IIR}(j\omega)$ and $C_{FIR}(j\omega)$; - -: $C_{FIR}(j\omega)$; —: $C_{IIR}(j\omega)$

$$C_{\mathrm{FIR}}(e^{j\omega}) = \frac{C(e^{j\omega})}{C_{\mathrm{IIR}}(e^{j\omega})}. \tag{23}$$

Figure 7 shows the frequency response functions of $C_{\mathrm{FIR}}(e^{j\omega})$ and $C_{\mathrm{IIR}}(e^{j\omega})$. Clearly, we can see that the gain of $C_{\mathrm{FIR}}(e^{j\omega})$ within control bandwidth is almost a constant, but otherwise is very high. It is then necessary to filter $C_{\mathrm{FIR}}(e^{j\omega})$ with a bandpass filter $W(e^{j\omega})$:

$$C'_{\mathrm{FIR}}(e^{j\omega}) = W(e^{j\omega})C_{\mathrm{FIR}}(e^{j\omega}). \tag{24}$$

Inverse Fourier transform of $C'_{\mathrm{FIR}}(e^{j\omega})$ gives the coefficients of the FIR filter. Finally, we form the controller $C'(e^{j\omega})$ by cascading $C'_{\mathrm{FIR}}(e^{j\omega})$ and $C_{\mathrm{IIR}}(e^{j\omega})$

$$C'(e^{j\omega}) = C'_{\mathrm{FIR}}(e^{j\omega})C_{\mathrm{IIR}}(e^{j\omega}). \tag{25}$$

Figure 8 shows the impulse responses of $C'_{\mathrm{FIR}}(e^{j\omega})$, $C_{\mathrm{IIR}}(e^{j\omega})$ and $C'(e^{j\omega})$. As expected, the length of the impulse response $C'_{\mathrm{FIR}}(e^{j\omega})$ is much shorter than the pure FIR implementation of Fig. 5(*b*).

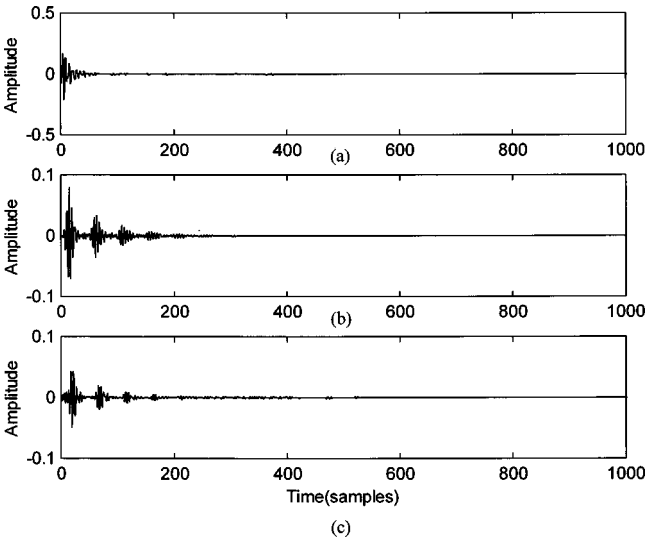

Fig. 8 Impulse response functions of hybrid implementation (*a*) $C'_{FIR}(j\omega)$, (*b*) $C_{IIR}(j\omega)$ (*c*) $C'(j\omega)$

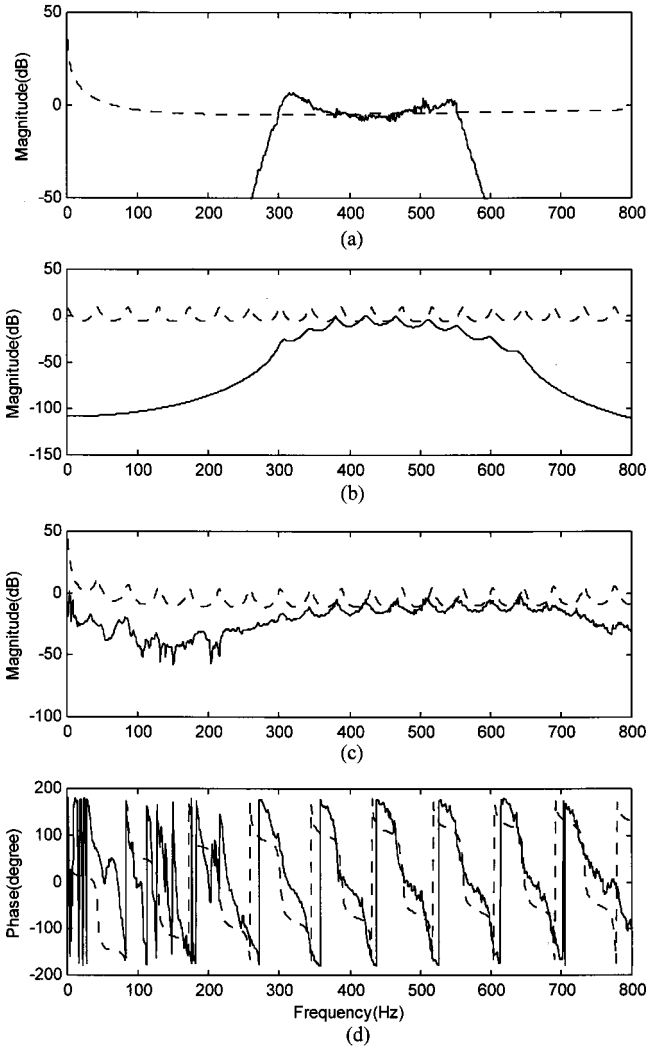

Fig. 9 Frequency response functions of hybrid implementation (*a*) magnitude of FIR part (*b*) magnitude of the IIR part (*c*) magnitude of the cascaded controller (*d*) phase of cascaded controller —: hybrid implementation of Roure's controller; - -: method of electro-mechanical constants of ideal controller

For reference, the frequency response functions between the method of electromechanical constants and the hybrid implementation are as we compared in Fig. 9. The FIR part and the IIR part indeed qualitatively reflect the characteristics of the transducer dynamics and the repetitive controller in the ideal controller. This result manifests the significance of finite source impedance that has been pointed out by Munjal and Eriksson [1] but overlooked by many other ANC researchers. Nevertheless, some errors can still be observed in both the magnitude and phase responses, which results in the failure of the method of electromechanical constants.

4 Experimental Verification

The experimental setup is shown in Fig. 10. A duct made of plywood (damping 0.04) is used for verifying the proposed ANC controllers. The dimensions of the duct and the locations of transducer are shown in the figure. The length of the duct is 440 cm, and the cross section is 25 cm×25 cm. The distance between measurement microphone and control speaker is set to be 379.5 cm such that the causality constraint can be met. The controllers are implemented on a TMS320C32 DSP. The sampling frequency is chosen to be 2k Hz.

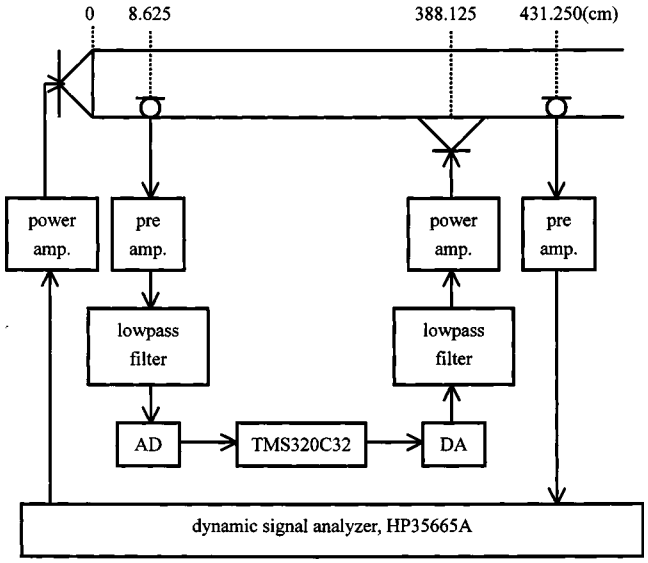

Fig. 10 The experimental arrangement

Some design considerations in practical implementation are summarized as follows. The gain level of the controller can be fine-tuned to improve performance (0.5~1.0). The length of the FIR filter is also a crucial factor. If the filter length is longer than 600, there will be a surge of control output when the controller is activated. Thus it is necessary to shorten the filter by, for example, direct truncation of the impulse response. Care should be taken to choose the filter length such that the frequency responses (especially the phase) of the DSP-implemented controller and the desired controller are accurately matched.

Considering the cutoff frequency of the duct and poor response of speaker at low frequency, we chose control bandwidth to be 300~600 Hz. Frequency windows have significant effect on performance. Without the window, the system may become saturated because of excessive control output. Two types of frequency windows are employed in the paper: a bandpass filter (300 ~600 Hz) and Wiener filter

$$C'_{FIR}(e^{j\omega}) = C_{FIR}(e^{j\omega}) \frac{1}{1+0.9|C_{FIR}(e^{j\omega})|^2}. \qquad (26)$$

The experimental results obtained from three approaches of filter implementation are summarized in Fig. 11 and Table 1. Total attenuation is the attenuation within the band 300~600 Hz. The hybrid implementation shows remarkable performance over the other two approaches: shorter FIR filter than the pure FIR implementation, smaller IIR filter order than the pure IIR implementation and the largest maximum attenuation (17.2 dB) and total attenuation (4.4 dB) among all implementations.

As mentioned previously, the ideal controller is robust in that it is independent of boundary conditions. We shall validate this point by closing the end of the duct by a rigid cap. Figure 12 shows the performance before and after closing the end. The system remains stable and noise attenuation can still be achieved by using the same controller after closing the end. Note, however, the amount of attenuation is different for two different end conditions.

The paper is not intended to overemphasize the superiority of any method over the others. Three approaches of implementing the ideal controller merely have different characteristics, as summarized in Table 2. The FIR implementation is straightforward and numerically stable, but often results in excessively long filters. IIR implementation requires only moderate order filter, provided finite word-length effects are properly taken care of. Hybrid implementation bears most physical insight of the ideal controller. Only a low order FIR filter pertaining to the transducer character-

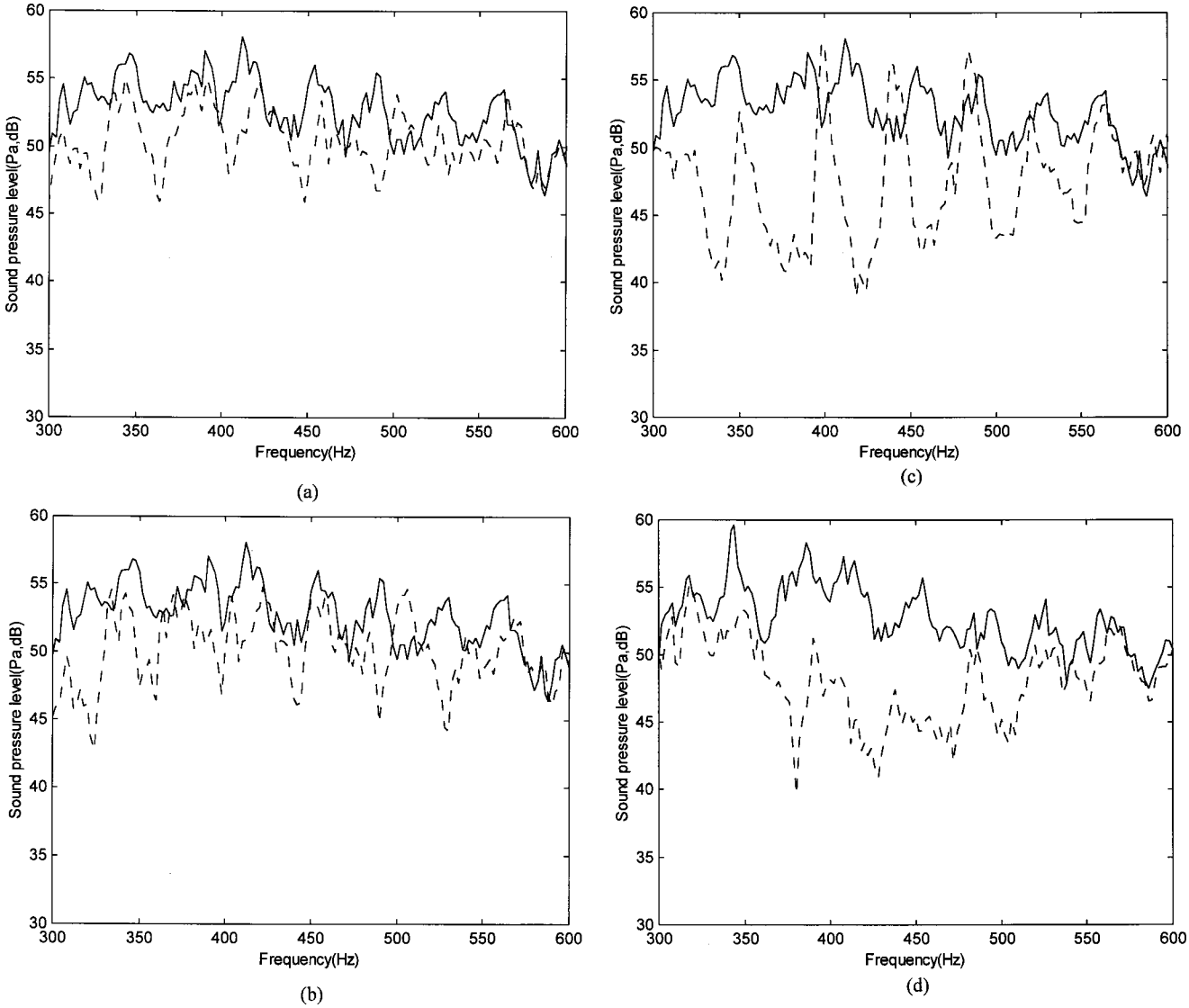

Fig. 11 Experimental results of active attenuation (*a*) FIR implementation (*b*) IIR implementation (*c*) hybrid implementation using bandpass filter (*d*) hybrid implementation using Wiener filter —: control off, - -: control on

istics and a low order IIR filter pertaining to the duct characteristics are needed in realizing the controller. This feature is particularly useful for applications where the system is lightly damped and transducers are omni-directional. It may appear from the comparison in Table 1 that hybrid implementation outperforms the other methods. As pointed out by the reviewer, the IIR filter should perform better than the hybrid filter if great care was taken to identify the filter coefficients. The experimental results did not

Table 1 Comparison of different implementations of the ideal controller

	FIR length	IIR order	Max. attenuation	Total attenuation
FIR	500	----	8.7 dB	2.4 dB
IIR	----	30	8.9 dB	2.5 dB
Hybrid-bandpass	50	18	17.2 dB	3.8 dB
Hybrid-Wiener	50	18	15.5 dB	4.4 dB

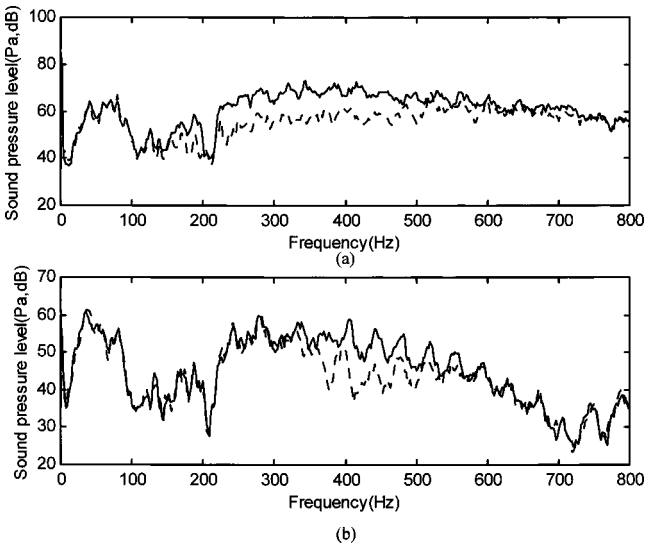

Fig. 12 Experimental results of active attenuation (*a*) open end (*b*) closed end —: control off - -: control on

Table 2 Summary of implementation methods of the spatially feedforward controller

	FIR	IIR	Hybrid
Filter coefficients	many	few	few
Stability requirement	always stable	could be unstable	could be unstable
Numerical problem	almost none	severe	medium
Physical insight	none	none	yes
Control bandwidth	wide	medium	medium
Performance	fair	good	good

agree well with the reviewer's comment which could be due to numerical difficulties in implementing the high order IIR filter (with 30 lightly damped poles).

5 Concluding Remarks

The ideal controller for broadband attenuation of noise in ducts, using spatially feedforward structure, is investigated on the basis of in-depth acoustic analysis and control engineering. The contribution of the paper is to unify the acoustic analysis of the ideal controller proposed by Munjal and Eriksson [1], and the system theoretic analysis of Hong and Bernstein [7] of the zero spillover controller first proposed by Roure [2]. The ideal controller is extended to a realizable controller in considering the transducer dynamics and design constraints involved in implementation. The modified controller is then implemented on a DSP platform, using a FIR filter, an IIR filter and a hybrid filter. Three approaches of implementing the ideal controller are verified and compared by experiments. The experimental results showed that the system achieved 17.2 dB maximal attenuation in the frequency band 300–600 Hz.

Along the same line of the preliminary results, future research will be focused on the following aspects. The method of electromechanical constants will be revisited such that digital implementation can be further simplified. Actions should be taken to shorten the impulse response of the controller. This can be done by two ways: lining the duct by absorbing materials (damping increased) and using directional transducer arrangement (acoustic feedback reduced). The robustness should be optimally accounted for by using more sophisticated algorithms, e.g., H_∞ instead of direct truncation of filters. For time-varying spatially feedforward problems, it is well known that the adaptive FIR filter (FXLMS) is ineffective and the adaptive IIR filter IIR (FULMS) occasionally has convergence problems [4]. This sheds some light on the hybrid implementation which requires only a low order FIR filter pertaining to the transducer characteristics and a low order IIR filter pertaining to the duct characteristics. In the future, the separablility of controller structure could possibly be exploited in adaptive implementation of the duct ANC system.

Acknowledgment

The work was supported by the National Science Council (NSC) in Taiwan, Republic of China, under the project number NSC 87-2212-E009-022.

References

[1] Munjal, M. L., and Eriksson, L. J., 1988, ''An Analytical, One-dimensional, Standing-Wave Model of a Linear Active Noise Control System in a Duct,'' J. Acoust. Soc. Am., **84**, pp. 1086–1093.
[2] Roure, A., 1985, ''Self-adaptive Broadband Active Sound Control System,'' J. Sound Vib., **101**, pp. 429–441.
[3] Elliott, S. J., and Nelson, P. A., 1993, ''Active Noise Control'' IEEE Signal Process. Mag., **10**, No. 4, pp. 12–35.
[4] Kuo, S. M., and Morgan, D. R., 1995, *Active Noise Control Systems: Algorithms and DSP Implementations*, Wiley, New York.
[5] Bai, M. R., and Lee, D. J., 1997, ''Implementation of an Active Headset by using the H_∞ Robust Control Theory,'' J. Acoust. Soc. Am., **102**, No. 4, pp. 2184–2190.
[6] MacMartin, D. G., and Hall, S. R., 1991, ''Structural Control Experiments Using and H_∞ Power Flow Approach,'' J. Sound Vib., **148**, No. 2, pp. 223–241.
[7] Hong, J., and Bernstein, D. S., 1998, ''Bode Integral Constraints, Colocation, and Spillover in Active Noise and Vibration Control,'' IEEE Control Syst. Tech., **6**, pp. 111–120.
[8] Desoer, C. A., and Kuh, E. S., 1969, *Basic Circuit Theory*, McGraw-Hill, New York.
[9] Clark, R. L., and Bernstein, D. S., 1996, ''Hybrid Control: Separation in Design,'' J. Sound Vib., **214**, No. 4, pp. 784–791.
[10] Bai, M. R., and Lin, Z., 1998, ''Active Noise Cancellation for a Three-dimensional Enclosure by Using Multiple-Channel Adaptive Control and H_∞ Control,'' ASME J. Vibr. Acoust., **120**, pp. 958–964.
[11] Tomizuka, M., Tsao, T. S., and Chew, K. K., 1989, ''Analysis and Synthesis of Discrete-time Repetitive Controllers,'' ASME J. Dyn. Syst., Meas., Control, **111**, pp. 353–358.
[12] Swinbanks, M. A., 1973, ''The Active Control of Sound Propagation in Long Ducts,'' J. Sound Vib., **27**, pp. 411–436.
[13] La Fontaine, R. F., and Shepherd, I. C., 1983, ''An Experimental Study of a Broadband Active Attenuator for Cancellation of Random Noise in Ducts,'' J. Sound Vib., **91**, No. 3, pp. 351–362.
[14] Beranek, L. L., 1996, *Acoustics*, Acoustical Society of America, Woodbury, NY.
[15] Bai, M. R., and Wu, H. P., 1998, ''Robust Control Design of a Sensorless Bass-enhanced Moving-Coil Loudspeaker System,'' J. Acoust. Soc. Am., **105**, pp. 3283–3289.
[16] Juang, J. N., 1994, *Applied System Identification*, Prentice-Hall, Englewood Cliffs, NJ.